Proceedings of FEDSM'98
1998 ASME Fluids Engineering Division Summer Meeting
June 21-25, 1998, Washington, DC

FEDSM98-4843

A COMBINED EXPERIMENTAL AND COMPUTATIONAL STUDY OF FLOWFIELDS IN LOUVERED FIN HEAT EXCHANGERS

Marlow E. Springer and Karen A. Thole*
University of Wisconsin
Mechanical Engineering Department
1513 University Avenue
Madison, WI 53706-1572

*Phone/Fax: (608)262-0923/(608)265-2316
Email: thole@engr.wisc.edu

L. Winston Zhang, Steve B. Memory and Jonathan P. Wattelet
Modine Manufacturing Company
Research and Development
1500 DeKoven Avenue
Racine, Wisconsin 53403-2552

ABSTRACT

This paper presents an experimental and computational study of flow through a louvered fin array at two different Reynolds numbers (Re_{L_p} = 230 and 1016 based on louver pitch, L_p, and inlet face velocity, U_{in}). The experimental work was conducted on a 20:1 scaled-up model of a 19-row louvered fin array with a louver angle (θ) of 27° and a fin pitch to louver pitch (F_p/L_p) of 0.76. The flowfield measurements were made using a two componet laser Doppler velocimeter (LDV). The computational simulations were performed for one louver row (same louver geometry) assuming periodic boundary conditions and two-dimensional, steady, laminar flow. In general, good agreement was found between the experimental measurements and computational predictions for all conditions. Bulk flow characteristics indicated that for the Reynolds numbers studied, the flow was louver directed and became fully-developed between the fourth and fifth louver. For the fully developed region, the flow entering the louver passage had remnants of the wake from the upstream louver. At the higher Reynolds numbers, the flow entering the passage was also affected by the wake from two louvers upstream.

INTRODUCTION

Louvered fin heat exchangers have been used extensively in automotive applications such as radiators, oil coolers, condensers and charge air coolers. The dominating thermal resistance in this type of heat exchanger is on the airside where the flow characteristics can be quite complex. Louvered fins are interrupted surfaces and are commonly used in heat exchanger designs for reasons beyond simply increasing the convective heat transfer surface area. These interruptions break up the growth of the laminar boundary layer that naturally forms along the louver, thereby forming a new boundary layer with an associated high heat transfer region. However, the formation of this fresh boundary layer along succeeding louvers can be greatly affected by the incoming flow from the upstream portion of the louver array.

To ultimately reduce the space, weight, and cost for louvered fin heat exchangers, one needs to improve the efficiency and quality control of air-cooled heat exchangers. Before any such optimization can take place, detailed studies are needed to provide a good understanding of the flows within the louvers and how they are affected for varying flow conditions and geometries.

This paper presents a two-pronged approach that compares computational fluid dynamics (CFD) predictions with LDV measurements in a 20:1 scaled up louver array. To the authors' knowledge, this is the first time that LDV has been used for such detailed measurements and the success of the study clearly demonstrates the feasibility and validity of doing so. Measurements were limited to steady laminar flows at low Reynolds numbers (Re_{L_p} = 230 and 1016). The CFD predictions employed a two-dimensional, steady, numerical simulation on one row of louvered fins with periodic boundary conditions.

RELEVANT STUDIES

Louvered fin studies date back to the flow visualization work performed by Beauvais (1965) using smoke traces. Based on his observations, Beauvais argued that the heat transfer in the first section of each louver can be treated as laminar flow over a flat plate, whereas further downstream, it can be approximated as laminar flow in a duct with a parabolic velocity distribution. Davenport (1983) performed flow visualization experiments identical to those of Beauavis and found the flow characteristics to be a function of Reynolds number. He also discovered that the friction factor

was close to that given by the Blasius solution for a flat plate at low Reynolds numbers but flattened at higher Reynolds numbers, where characteristics of both friction and form drag were evident. The heat transfer and pressure drop studies by Achaichia and Cowell (1988a) also identified two types of flow conditions dependent on the Reynolds number, a 'duct' and 'louver' directed flow at low and high velocities respectively. However, at high Reynolds numbers, they found the Stanton number was parallel to, but lower than that of laminar boundary layer flow over a flat plate while at low Reynolds numbers, the Stanton number showed similar characteristics to that of laminar duct flow.

Webb and Trauger (1991) performed flow visualization in louvered fins using a dye injection technique for a Reynolds number range of 400 to 4000. They defined a dimensionless quantity called "flow efficiency" given as the ratio of mean flow angle to louver angle. For a given set of geometrical parameters, the flow efficiency increased with the Reynolds number. The only detailed flowfield measurements given in the open literature were performed by Antoniou et al. (1990) who used a hot-wire anemometer in a 16:1 scaled up louver array model. They presented flowfield results for three different Reynolds numbers ranging from 500 to 2300 ($\theta = 25°$, $F_p/L_p = 1.69$). Their results indicated an increase in the mean flow angle for each stream-wise louver until approximately the fourth louver position. Beyond the fourth louver, the mean flow angle approached 92% of the louver angle over the range of Reynolds numbers investigated. Downstream of the turning louver, the flow took longer to re-adjust, particularly at lower Reynolds numbers.

With regard to computational work, Achaichia and Cowell (1988b) simulated flow through a louvered fin array by modeling a fully-developed, steady, laminar flow over a number of single louvers (θ = 15-55°, F_p/L_p = 1.0-2.5), with periodic boundary conditions in both directions. Their analysis showed that as the Reynolds number increased, the mean flow angle approached the louver angle to within a few degrees. Zhang (1996) simulated both steady and unsteady flow over a single louver using the same periodic domain ($\theta = 25°$, $F_p/L_p = 1.25$) and found similar results. In addition, at high Reynolds numbers ($Re_{Lp} > 782$), Zhang also predicted vortex shedding from both front and back leading edges of the louver.

Using simple geometric analysis, Suga and Aoki (1991) proposed a simple expression to represent the optimum geometric relation between θ and (F_p/L_p) by controlling the distribution of the thermal wake produced from an upstream louver:

$$F_p/L_p = 1.5 \tan\theta \qquad (1)$$

This equation was 'verified' using numerical techniques. They found that their heat transfer results were independent of Reynolds number for the range they considered ($64 < Re_{Lp} < 450$). The present louver array geometry ($F_p/L_p = 0.76$) was 'predicted' using equation (1) based on a louver angle of 27°.

There is clearly a need for more detailed flowfield measurements and a direct comparison between theory and experiment. LDV provides a means to obtain these detailed experimental measurements. To date there have been no direct comparisons between LDV measurements and CFD predictions for flows through louvered fins.

EXPERIMENTAL AND NUMERICAL APPROACHES

The studies discussed in this section deal with a louvered fin-and-tube design as illustrated in Figure 1a. The main focus is on the louvered fin array with the geometrical parameters of interest illustrated in Figure 1b. Table 1 summarizes the louvered fin geometry.

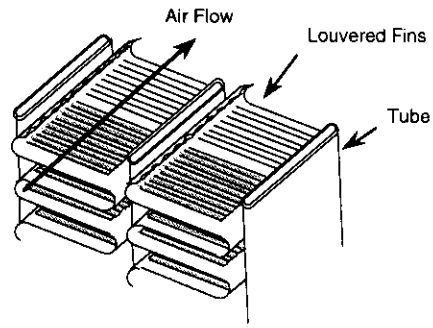

Figure 1a. Schematic of louvered fin-and-tube heat exchanger

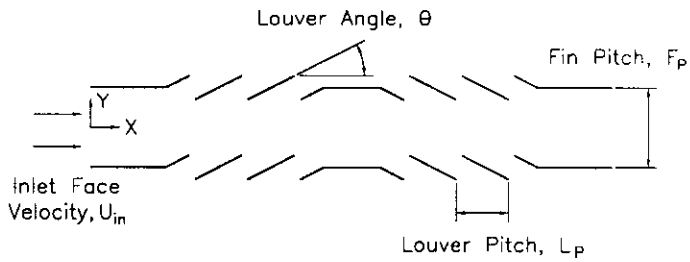

Figure 1b. Side view of louvered fin geometry

NOMENCLATURE

H = vertical distance between louvers, $H = F_p - t/\cos\theta$
F_p = fin pitch
L_p = louver pitch
Re_{Lp} = Reynolds number, $Re_{Lp} = U_{in}L_p/\nu$
t = fin thickness
u = streamwise velocity component
U = total velocity magnitude
U_{in} = inlet face velocity to test section
v = vertical velocity component
X = streamwise coordinate direction
Y = vertical coordinate direction relative to louver
α = flow angle, $\alpha = \tan^{-1}(v/u)$
ν = air viscosity
θ = louver angle

Table 1. Summary of Louvered Fin Geometry

Louver Angle (θ)	27°
Fin Pitch to Louver Pitch (F_p / L_p)	0.76
Fin Thickness to Louver Pitch (t / L_p)	0.08
Number of Louvers	17

For the experiments, a 20:1 scaled up model was placed in the test apparatus shown in Figure 2. Upstream of the test section there was a settling chamber to condition the flow entering the test section. At the entrance to the test section, screens and foam were used to straighten the incoming flow and achieve good flow uniformity with reduced turbulence levels. The flow was driven by a 12 W (1/64 HP) in-line axial fan running at 3500 RPM. A manual butterfly valve was used to control the flow rates to achieve the required inlet flow Reynolds numbers. Due to the blockage caused by the fin thickness, velocities entering the louver passage would be expected to be 12% higher than the inlet face velocity.

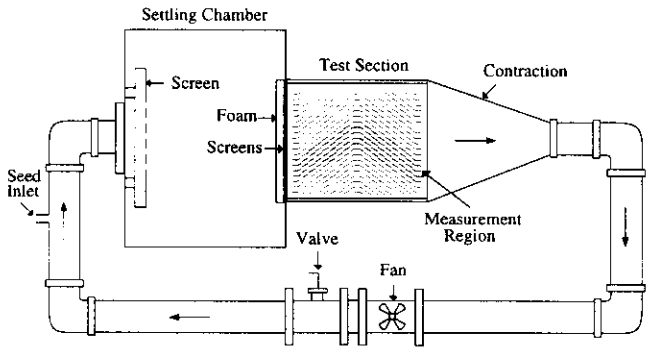

Figure 2. Flow loop for scaled-up louver experiments

To provide enough louver rows to ensure a periodic flow in a number of the passages, the test section was designed using CFD (Springer and Thole, 1998). Nineteen louver rows were found to be sufficient in that they provided approximately four louver passages (shown shaded in Figure 2) through which the flow was predicted and experimentally verified to be periodic. In addition, the location of the top wall was placed $3F_p$ away from the top row of louvers and the bottom wall was placed $0.5F_p$ from the bottom row. A larger spacing was needed on the top wall to allow the flow to enter straight into the upper portion of the louver array. The dimensions of the scaled up test section were 17.5 cm deep, 44.1 cm high and 69.6 cm long.

To avoid the boundary layer that formed on the test section walls, the velocity measurements were made approximately 25.4 mm into the depth of the test section from the sidewall. Flowfield measurements were first made across the depth of the test section to ensure that the measurements reported in this paper were not influenced by the sidewall boundary layer. Typical operating temperatures were maintained at 24 °C ± 1 °C.

A two component LDV system was used to measure the mean velocities in the louvered fin array. The focal length of the lens is 350 mm, with a probe volume that is 90 μm in diameter and 1.3 mm in length. Incense smoke was used as LDV seed particles, which were generated outside the main loop and injected just upstream of the settling chamber. Mean horizontal and vertical velocity components were obtained by sampling 5,000 points taken over a 15 to 20 second period at each measurement location. The bias uncertainty in the velocity measurements is estimated as 1%, arising from uncertainties in the Doppler frequencies and the fringe spacing. The velocity precision error, with a 95% confidence interval, is a maximum of 0.1%. The estimated uncertainties in the measured flow angle, obtained from the measured velocity components, were 1.7%.

Figure 3 shows three rows of louvers in the test section and the positions at which velocity profiles were measured (referred to as 'cuts'). It was only possible to measure the components in 75% of the louver passage (i.e. the bulk flow) before the laser beams were blocked by neighboring louvers at a position inside the passage that was out of the side-wall boundary layer. At the inlet louver, cuts were taken at the center of the horizontal portion (cut 1a) and at the center of the angled portion (cut 1b) in the stream-wise direction. The cut for the second louver was at the center in the stream-wise direction (cut 2). Five cuts were taken in the fifth louver (cuts 5a-e) to document the flow as it passes through a passage where the flow is considered to be "fully-developed". In addition, five cuts were also taken in the thirteenth louver (cuts 13a-e) which is the mirror image of the fifth louver with respect to the turning louver.

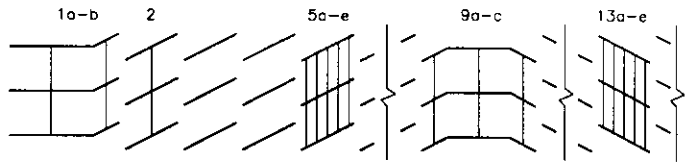

Figure 3. Louver orientation and measurement cut locations

The computations were performed using a CFD package (FLUENT/UNS), which adopts a pressure-based, finite volume scheme. The flow for all of the computations presented in this paper was considered to be two-dimensional, steady, and laminar. The computational domain considered was limited to one complete row (17 louvers) with periodic boundary conditions top and bottom, a fixed inlet velocity located at $1.5L_p$ upstream of the first louver and an outlet boundary set at $7L_p$ downstream of the last louver. The grid was generated using the code's unstructured triangular mesh generator. The discretized equations were solved using the SIMPLE algorithm with second order accuracy.

Grid independence was achieved through both grid adaption and grid resolution studies. After each refinement based on velocity gradients in the solution, the grid was further refined to reduce the change in cell volumes between adjacent cells. These steps were followed as the Reynolds number was incrementally increased to a maximum of 1016. Figure 4 shows normalized predictions of velocity profile against louver passage traverse (given as U/U_{in} versus Y/H) at cut 5c for a Reynolds number of

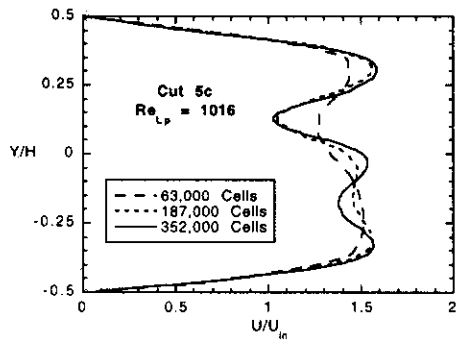

Figure 4. Velocity magnitude profile at cut 5c using different computational domain sizes

1016 for three different grid sizes. Clearly the smallest grid size of 63,000 cells was not sufficient to resolve the flow, although the grid had been adapted according to the velocity gradients. At the next resolution (grid size of 187,000 cells), it can be seen that the flow was qualitatively well resolved. The maximum change in velocity magnitude associated with this grid increase was 19%. Increasing the grid size further (to 352,000 cells) resulted in a further 5.5% maximum change in velocity. A similar grid independence study was conducted for Re_{Lp} = 230, providing a final grid size of 291,000 cells.

BULK FLOW CHARACTERTICS

This section discusses the development of the bulk flow as it passes through the inlet louvers and becomes fully-developed further downstream. As mentioned above, profiles normal to the flow direction of the streamwise and vertical velocity components were measured at the inlet (first), second, and fifth louvers. Figures 5a and 5b compare predicted and experimental normalized velocity profiles and ratios of local flow angle to louver angle for Re_{Lp} = 230 for the inlet and second louver, i.e. in the developing flow region. Figures 6a and 6b show the same information for Re_{Lp} = 1016. Note that the local flow angle (α) was calculated using $\alpha = \tan^{-1}(v/u)$. The mean flow angles discussed later in this section are based on an integrated average of the local values measured over 75% of the passage. Figures 7a and 7b show the profiles at cut 5c for both Reynolds numbers.

At cut 1a (inlet louver), the figures show that the flow is basically uniform and is directed essentially in the streamwise direction (mean $\alpha/\theta < 0.1$). At Re_{Lp} = 230, the core flow of the passage has been accelerated to $1.4U_{in}$, while at Re_{Lp} = 1016, it is only $1.2U_{in}$. This higher acceleration at the lower Reynolds number is due to the thicker boundary layers that have formed on the louvers. As stated earlier, based on the total inlet to passage area ratios, one would expect that the flow in the passages would only be 12% higher. The CFD predictions are seen to be in good agreement with the measured profiles and local flow angles at this cut with only slightly higher velocities predicted than measured for Re_{Lp} = 1016. These

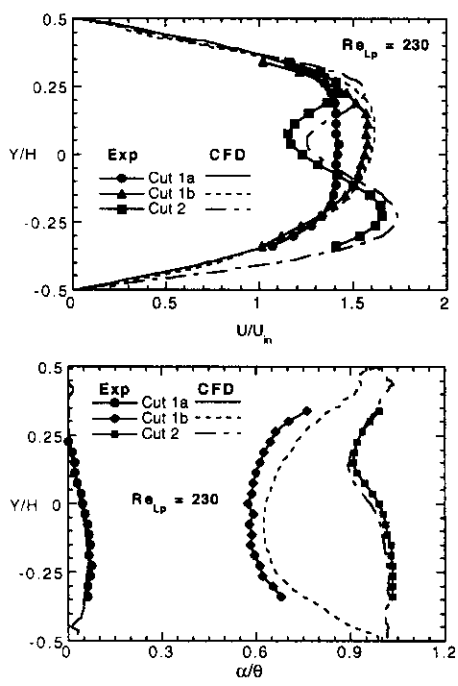

Figure 5a, b. Velocity magnitude and ratio of local flow angle to louver angle showing development of bulk flow at Re_{Lp} = 230

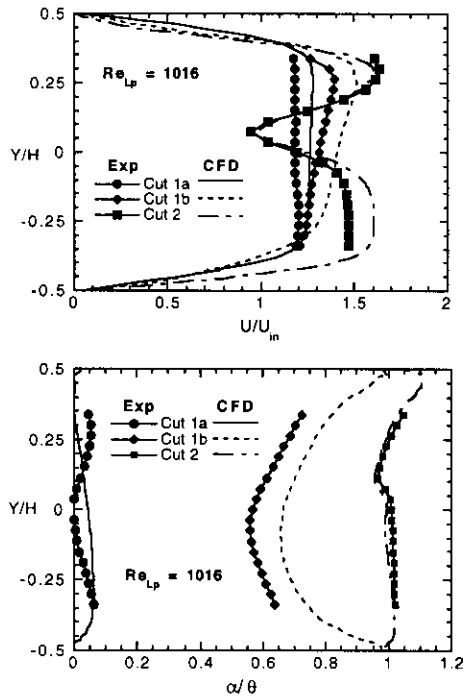

Figure 6a, b. Velocity magnitude and ratio of local flow angle to louver angle showing development of bulk flow at Re_{Lp} = 1016

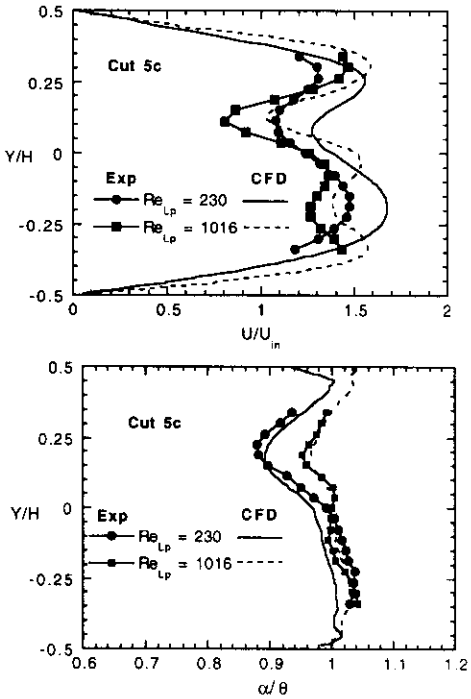

Figure 7a, b. Velocity magnitude and ratio of local flow angle to louver angle for fully-developed flow in fifth louver at Re_{Lp} = 230 and 1016

differences can be attributed to there not being an infinite number of rows in the experimental model. The lower louvers of the model near the turning louver are not fed by upstream louvers. This effect propagates upward causing lower speed fluid in the measurement region. Note that the effect is worse at cut 5c than at the inlet, consistent with the lower louvers providing little flow.

For cut 1b, the flow begins to be directed by the louver. At this location for both Reynolds numbers, prediction and measurement indicate that the velocity is beginning to show a non-uniform character, with higher velocities near the top of the passage where the flow does not experience blockage from the second half of the first louver. Measured mean ratios of flow angle to louver angle around $\alpha/\theta = 0.6$ are seen for both Reynolds numbers, with the CFD predictions indicating slightly higher values.

The flow has changed significantly by the second louver (cut 2) showing not only wake effects of the upstream louver, but also that it is mostly louver directed flow, even for the lower Reynolds number. At this position, there is a velocity defect at $Y/H \approx 0.10$ for both Reynolds numbers due to the upstream louver. The minimum velocity at $Re_{L_p} = 230$ is $1.15U_{in}$, while a stronger velocity deficit exists at $Re_{L_p} = 1016$ of $0.95U_{in}$. As expected, the wake region is also narrower at $Re_{L_p} = 1016$. In each case, the CFD predictions indicate this deficit nicely, although the peak magnitude is predicted to be up to 17% higher.

The ratios of local flow angle to louver angle for cut 2 show that the flow is essentially louver directed, with a mean $\alpha/\theta \approx 0.98$ for $Re_{L_p} = 230$ and 1.0 for $Re_{L_p} = 1016$. For the low Reynolds number at this cut, the flow is directed closer to the louver angle in the lower portion of the passage than in the upper portion. This can be explained if one looks at the local flow angles that leave the upstream louver passage. Again, the CFD predictions are very close to the experimental results.

In the fifth louver passage (cuts 5a-e), the flow has reached a fully-developed condition for both Reynolds numbers. Figures 7a and 7b compare predicted and experimental normalized velocity profiles and ratios of local flow angle to louver angle for both Reynolds numbers at cut 5c. Note that there is not much change in the shape of the profile between the second and fifth louvers at $Re_{L_p} = 230$. There is a large difference, however, between these two louvers for $Re_{L_p} = 1016$. An additional velocity deficit has appeared near the bottom of the fifth louver ($Y/H \approx -0.2$) which is not apparent at the second louver. If one looks at Figure 3, it can be seen that this additional velocity deficit within the fifth louver is due to the wake of the third louver (two louvers upstream). This secondary wake is much smaller than the primary wake of the immediate louver upstream (in this case the fourth louver) as expected. The minimum velocity in the main wake region is $0.8U_{in}$ while it is $1.25U_{in}$ in the secondary wake region. CFD predictions indicate the single deficit for $Re_{L_p} = 230$ and the double deficit for $Re_{L_p} = 1016$ very well, although the magnitudes are still higher than those measured. The shape of the α/θ profile is quite similar to the second louver profile, with the mean being around 1.0. However, there is a discernable decrease in the local flow angle in the region of the velocity deficit, becoming more apparent for lower Reynolds number. This is due to a thicker boundary layer associated with the lower Reynolds number. Again, the CFD predictions indicate the forms of these profiles very well.

Figures 8a and 8b show the detailed measured and predicted velocity vectors for $Re_{L_p} = 230$ taken from the equally spaced cuts (at $0.18L_p$) in the streamwise direction through the fifth louver passage (cuts 5a-e). Figures 9a and 9b show the same details for $Re_{L_p} = 1016$. Note that the CFD predictions include the boundary layer as well and show the flow separation that was discussed earlier for $Re_{L_p} = 1016$. The velocity deficit caused by the wake from the louver immediately upstream is clearly seen for both Reynolds numbers. However, the velocity deficit from the second louver upstream is only visible at $Re_{L_p} = 1016$, clearly at cut 5a, but diminishing to a fairly flat profile by cut 5e. At the passage entrance near the upper louver, the flow is directed at an angle substantially less than the louver angle, but approaches the louver angle as one moves further downstream ($\alpha/\theta \rightarrow 1$). This deflection is stronger at $Re_{L_p} = 230$, where the boundary layer is much thicker.

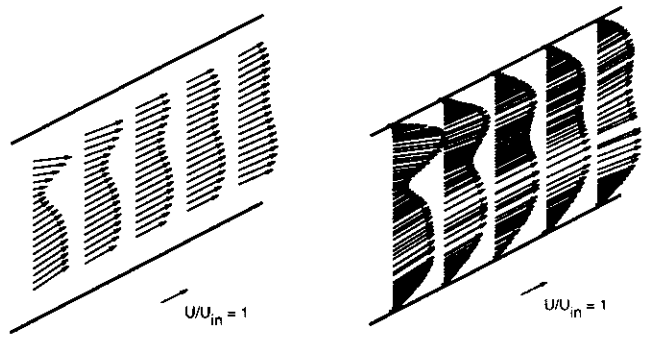

Figure 8a,b. Measured and predicted velocity vectors in the fifth louver passage at $Re_{L_p} = 230$

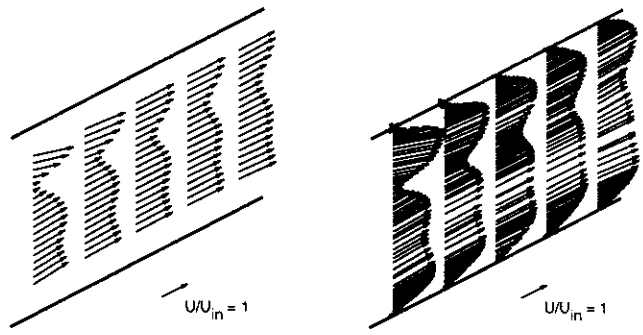

Figure 9a,b. Measured and predicted velocity vectors in the fifth louver passage at $Re_{L_p} = 1016$

Figure 10 shows measured velocity vectors at three positions within the passage of the middle turning louver (ninth louver) at $Re_{L_p} = 1016$. The flow in the upstream portion of the passage (cut 9a) is very similar to the flow through the fifth louver, exhibiting velocity deficits from the two immediate upstream louvers. The minimum velocity is $0.55U_{in}$ in the primary wake and $1.22U_{in}$ in the

secondary wake. The local velocity vector angles are starting to be affected by the turn and the mean α/θ is only 0.79 at this position. Within the horizontal portion of the louver (cut 9b), the effects of the upstream louvers have diminished, but are still evident. The minimum velocity is now $0.9U_{in}$ in the primary wake and $1.26U_{in}$ in the secondary wake. The flow is almost horizontal, with a mean α/θ of only 0.1, similar to the inlet louver. In the downstream portion of the louver passage (cut 9c), the velocity deficits have almost disappeared and the profile is similar to that seen in cut 1b. At this position, the velocity angles are also very close to what they were at cut 1a, with a mean α/θ of 0.64. The flow angle is now closer to the louver angle in the lower portion of the passage. This is due to a greater flow resistance in the upper portion of the passage, in turn due to the thicker boundary layer and the leading edge of the next louver downstream.

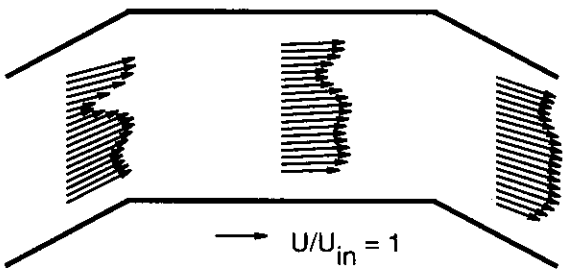

Figure 10. Measured velocity vectors in the turning louver at Re_{Lp} = 1016

Figure 11 shows measured velocity vectors from the five cuts made in the thirteenth louver passage (cuts 13a-e). The flow through this passage is approximately a mirror image of that through the fifth louver passage. The main differences are due to the orientation of the upstream louvers, i.e. the geometry of the louver array itself. The velocity deficit from the wake of the first louver upstream is now in the lower portion of the passage, and that from the second louver upstream is now in the upper portion. With this difference in mind, the behavior of the fluid

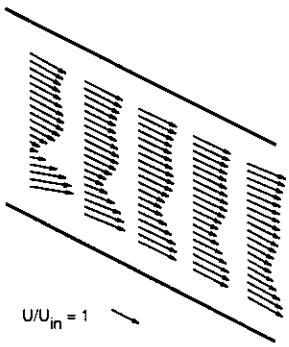

Figure 11. Measured velocity vectors in the thirteenth louver passage at Re_{Lp} = 1016

in the fifth and thirteenth louver passages is almost identical. The overall velocity has decreased slightly due to the pressure drop as the flow progresses through the louver array. Finally, the mean flow to louver angle is approximately 0.94 through this passage, similar to that found in the fifth louver passage.

CONCLUSIONS

The feasibility of using the LDV technique for detailed flow measurements in a scaled up louvered fin array has been shown to be successful. Furthermore, good agreement has been obtained between these measurements and predicted results using CFD. For the two Reynolds numbers studied (Re_{Lp} = 230 and 1016), the flow was found to be louver directed and became fully-developed by the fifth louver of a seventeen louver array. For fully-developed flow, remnants of the wake from the immediate upstream louver for both Reynolds numbers were evident. At Re_{Lp} = 1016, the flow entering the passage was also affected by the wake from two louvers upstream. The qualitative form of the CFD predictions was very good for the bulk flow, indicating the velocity deficits accurately. However, the predicted quantitative velocities were slightly higher than measured.

REFERENCES

Achaichia, A. and Cowell, T. A., 1988a, Heat Transfer and Pressure Drop Characteristics of Flat Tube and Louvered Plate Fin Surfaces, *Experimental Thermal Fluid Science*, vol. 1, pp. 147-157.

Achaichia, A. and Cowell, T. A., 1988b, A Finte Difference Analysis of Fully Developed Periodic Laminar Flow in Inclined Louvered Arrays, *Proceedings of 2nd UK National Heat Transfer Conference*, Glasgow, vol. 2, pp. 883-888.

Antoniou, A. A., Heikal, M. R., and Cowell, T. A., 1990, Measurements of Local Velocity and Turbulence Levels in Arrays of Louvered Plate Fins, *Heat Transfer*, Paper No. 10-EH-18, pp. 105-110.

Beauvais, F. N., 1965, An Aerodynamic Look at Automobile Radiators, SAE Paper No. 650470.

Davenport, C. J., 1983, Correlations for Heat Transfer and Flow Friction Characteristics of Louvered Fin, Heat Transfer - Seattle 1983, AICHE Symposium Series, No. 225, vol. 79, pp. 19-27.

Springer, M. and Thole, K. A., 1998, Experimental Design for Flowfield Studies of Louvered Fins, under review for the *Experimental Thermal and Fluid Science.*

Suga, K. and Aoki, 1991, H., Numerical Study on Heat Transfer and Pressure Drop in Multilouvered Fins, *ASME/JSME Thermal Engineering Proceedings*, Vol. 4, pp. 361-368.

Webb, R. L. and Trauger, P., 1991, Flow Structure in the Louvered Fin Heat Exchanger Geometry, *Experimental Thermal and Fluid Science*, Vol. 4, pp. 205-217.

Zhang, L. W., 1996, A Numerical Study of Flow and Heat Transfer in Compact Heat Exchanger, Ph.D. Thesis, University of Illinois at Urbana-Champaign, Urbana, Illinois.